Ionization of large-scale absorbing haloes and feedback events from high-redshift radio galaxies

L. Binette¹, R. J. Wilman², M. Villar-Martín³, R.A.E. Fosbury⁴ M. J. Jarvis⁵ and H. J. A. Röttgering⁶

- ¹ Instituto de Astronomía, UNAM, Ap. 70-264, 04510 México, DF, México
- ² Department of Physics, University of Durham, South Road, Durham DH1 3LE, UK (e-mail: r.j.wilman@durham.ac.uk)
- ³ Instituto de Astrofísica de Andalucía, CSIC, Apdo. 3004, 18080, Granada, Spain
- ⁴ ST-ECF, Karl-Schwarzschild Strasse 2, D-85748 Garching bei München, Germany
- ⁵ Astrophysics Department, Keble Road, Oxford OX1 3RH, UK
- ⁶ Leiden Observatory, P. O. Box 9513, 2300 RA Leiden, The Netherlands

Received February 2006/ Accepted

ABSTRACT

Aims. We present photoionization calculations for the spatially extended absorbers observed in front of the extended emission line spectrum of two high redshift radio-galaxies: 0943–242 ($z_{\rm e}=2.922$) and 0200+015 ($z_{\rm e}=2.230$), with the aim of reproducing the absorber column ratio, $N_{\rm CIV}/N_{\rm HI}$.

Methods. We explore the effects of using different UV continua in the photoionization calculations. A comparison is drawn between the absorber in 0200+015 and the two absorbers observed near the lensed Lynx Arc Nebula at redshift 3.36, which present very similar $N_{\rm CIV}/N_{\rm HI}$ ratios.

Results. We find that hot stars from a powerful starburst, or a metagalactic background radiation (MBR) in which stars dominate over quasars, are equally successful in reproducing the observed $N_{\rm CIV}/N_{\rm HI}$, assuming subsolar gas metallicities for each absorber. These softer SEDs eliminate the difference of a factor 1000 in metallicity between the two absorbers encountered in earlier work where a powerlaw SED was assumed. The detection of continuum flux in 0943–242 suggests that the level of ionizing photons is consistent with a stellar ionizing source.

Conclusions. If the MBR is responsible for the ionization of the radiogalaxy absorbing shells, their radii (if spherical) would be large (> 100 kpc) and their mass would be huge > $10^{12} \, \mathrm{M}_{\odot}$, implying that the feedback mechanism initiated by the central galaxy has caused the expulsion of more baryonic mass than that left in the radiogalaxy. If, as we believe is more likely, stellar ionizing sources within the radio galaxy are responsible for the absorber's ionization, smaller radii of $\sim 25 \, \mathrm{kpc}$ and much smaller masses ($\sim 10^8 - 10^{10} \, \mathrm{M}_{\odot}$) are inferred. This radius is consistent with the observed transition in radio source size between the smaller sources in which strong H_I absorption is almost ubiquitous, and the larger sources where it is mostly lacking. Finally, we outline further absorption line diagnostics which could be used to constrain further the properties of the haloes and their source of ionization.

Key words. Cosmology: early Universe – Galaxies: active – Galaxies: formation – Galaxies: ISM – Line: formation

1. Introduction

A prominent characteristic of high-redshift radio-galaxies (HzRGs) at z>2 is their spatially extended line emission regions (hereafter EELR), which are often luminous in Ly α (> $10^{44}\,\mathrm{erg\,s^{-1}}$) and extended over several to tens of kpc. The excitation mechanism for the *emission gas* is either shock excitation by jet material or AGN photoionization (the presence of N $\nu\lambda$ 1240 line emission precludes stellar photoionization). The EELR is kinematically active, with FWHM reaching 1000 km s⁻¹. With observations of a sample of HzRGs, Van Ojik et al. (1997;VO97) discovered that,

when observed at intermediate resolution (1–2 Å), the majority of HzRGs with small radio source sizes (< 50 kpc) exhibit narrow Ly α H I absorption. This absorption is superimposed upon the Ly α emission with a spatial extent comparable to that of the EELR. In addition to Ly α , the C IV $\lambda\lambda1549$ doublet has also been observed in absorption in two HzRGs, superimposed on the C IV emission line, firstly in 0943–242 ($z_{\rm e}=2.922$) (Binette et al. 2000, hereafter B00) and secondly in 0200+015 ($z_{\rm e}=2.230$) (Jarvis et al. 2003, hereafter J03). Building on the results of B00 and J03, in the present paper we examine the excitation mechanism of the large scale absorbing haloes in greater

detail by exploring photoionization by a variety of different spectral energy distributions (hereafter SED).

The basic structure of the paper is as follows. In the remainder of section 1 we review our current understanding of Hzrg absorbers, focusing on the distribution, ionization and metallicity of the absorbing gas and the specific problems which motivate our current study; an insightful comparison is made with the absorbers in the Lynx Arc Nebula (LAN), a gravitationally-lensed HII galaxy at z = 3.357. In section 2 we summarise the observational results we aim to reproduce, namely the $N_{\rm CIV}/N_{\rm HI}$ ratio in the aforementioned HzRGs and the LAN. Section 3 describes the MAPPINGS Ic code and our assumptions concerning the photoionizing SEDs. Section 4 presents the results of these calculations and in section 5 we assess their implications for the origins of the absorbers and their compatibility with other observables. Finally, in section 6 we present some additional absorption line diagnostics which may in future help to discrimate between the proposed scenarios.

1.1. Shell-like structure for the HzRG haloes

Among the HzRGs with small radio sources (< 50 kpc), the detection rate of associated absorption systems is 90% (9 out of 10 Hzrgs in the V097 study) while it is only 25% for larger radio-sizes. The fact that the absorption extends over the whole background EELR emission favours a shelllike geometry for the absorption systems rather than a conglomerate of individual clouds, as proposed initially by VO97. In Sect. 1.3 we give further indications as to why we retain the simplifying assumption of a simple shell structure in the current work. Because the density per unit redshift of the strong absorbers $(N_{\rm HI} > 10^{18} \, {\rm cm}^{-2})$ around HzRGs was found to be much higher than that given by the statistics of intergalactic medium (IGM) absorbers at large, VO97 inferred that they belong to the environment of the parent HzRG rather than to the IGM. The density of the thinnest absorbers ($< 10^{15} \,\mathrm{cm}^{-2}$) around HzRGs on the other hand is comparable to that of Ly α forest absorbers in the IGM, as more recently shown by Wilman et al. (2004: W04). It is conceivable that the physical conditions in the thin 1 HzRG absorbers are indistinguishable from those operating within typical IGM Ly α forest absorbers. The available data, however, are still insufficient to confirm or refute this proposition.

The rarity of absorbers among HzRGs with radio-sizes larger² than 50 kpc suggests that the typical lateral dimensions of the shell (in the plane of the sky) might be $\lesssim 50$ kpc. The proposed interpretation is that, as the AGN jet expands beyond such size, the bow-shocks overtake the shells and disrupt them. This is the first scenario, which we label A or "inner shell scenario". If valid, it suggests

that the expansion of the AGN jet cocoon is not the mechanism by which the shells are formed, but rather by which they are destroyed. Scenario A favours a shell formation mechanism that relies on large-scale outflows generated by episodes of massive star formation. Using high dispersion data from VLT-UVES, W04 proposed that the absorbers in HzRGs probably lie within the core of young galactic protoclusters, consistent with observations of their environments (e.g. Venemans et al. 2005; Overzier et al. 2006), and may be a byproduct of massive galaxy formation. Krause (2005) published hydrodynamical simulations of the formation of a shell due to the expansion of a stellar wind bow-shock. At a later stage in his model, an AGN jet is launched and a jet cocoon builds up. Once the jet has extended beyond the initial bow-shock, the jet cocoon destroys the shell as it overtakes it. An estimate of the timescale for this to occur can be obtained if one follows the reasoning of J03, where the radio-size represents a kind of internal clock (see Sect. 1.5), which characterizes not only the radio jet's age but also that of the starburst superwind that generates the shells.

A second possibility is that the rarity of shells among HzRGs with large radio-sizes may reflect an older phase in which the shells have expanded further out and thinned out considerably. This process would eventually render them undetectable (using the VO97 detection technique) when their $N_{\rm HI}$ columns drops below $\lesssim 10^{13}\,{\rm cm}^{-2}$. This is the second scenario, which we label B or "aging shell scenario". In this case, the distance between the shell and the parent HzRG is unknown and can be much larger than the upper limit size implied by scenario A, as will be discussed in 5.1. Scenario B leaves the possibility open that some of the shells may result from the expansion of a jet bow-shock (e.g. Krause 2002), although the most likely formation mechanism of the shells remains stellar superwind, as in scenario A.

The large scale Hzrg absorbers might be analogous to the absorbers detected within 3 20–50 h^{-1} kpc of high redshift galaxies, by Adelberger et al. (2005) using nearby-field spectroscopy of background QSOs or galaxies. The advantage of Hzrg absorber studies is that the intrinsic shell outflow velocity is more readily available from observations, but not their distance from the parent Hzrg (the reverse applies to the technique used by Adelberger et al., assuming spherical expansion of the absorbers).

The Hzrg shells share many similarities with at least some of Ly α -emitting 'blobs' (hereafter LAB; Steidel et al. 2000) associated with Lyman Break Galaxies (Pettini et al. 2001), and which are characterized by an EELR that can reach large sizes of up to $\sim 100\,\mathrm{kpc}$. An important difference is that the radio luminosities are much fainter or undetected in the latter case. Using integral field spectroscopy, Wilman et al. (2005) observed the Ly α -emitting 'blob' LAB-2 in the SSA22 protocluster at $z_\mathrm{e}=3.09$; they discovered a foreground absorber ($N_\mathrm{HI}\simeq 10^{19}\,\mathrm{cm}^{-2}$) with remarkable velocity coherence over a projected size of

¹ By "thin" we refer to a small H_I column density, not to a small physical size.

² VO97 (p. 369) showed that this finding is not the result of a selection effect due to the fact that larger radio sources have a narrower Ly α emission profile.

Where $h = H_o/100 \, \text{km s}^{-1} \, \text{Mpc}^{-1}$.

 $\sim 76 \times 26\,\mathrm{kpc}$. Their interpretation is that a galaxy-wide superwind has swept up $\sim 10^{11}\,\mathrm{M}_{\odot}$ of diffuse material from the IGM over a few 10^8 yr. This is a manifestation of the 'feedback' mechanism thought to be regulating the formation of galaxies.

1.2. What is ionizing the large scale haloes?

At least a fraction of the known haloes appear to be highly ionized. In both HzRGs in which a C IV $\lambda\lambda$ 1549 doublet has been observed in absorption (0943–242 and 0200+015), the absorption redshift corresponds to one of the Ly α absorbers. These two absorbing haloes therefore contain ionization species up to at least C⁺³. B00 and J03 assumed that the H I and C IV absorption species occur within a physically contiguous structure, an aspect discussed further in Sect. 1.3.

The possibility that the HzRG absorbing haloes are photoionized by the hidden nuclear radiation can be ruled out. Firstly, because there no observed continuum of sufficient strength underlying the EELR. This is as expected in the quasar-radio-galaxy unification picture (Barthel 1989; Antonucci 1993; Haas et al. 2005), in which the nuclear ionizing radiation is collimated along two ionization cones, which in radio-galaxies lie along the plane of the sky, and is therefore invisible to the observer and presumably to the intervening absorbers as well, unless rather contrived gas geometries are postulated. Secondly, B00 showed that the $C_{IV}/L_{y\alpha}$ emission- and absorption-line ratios in 0943–242 could not be reconciled with any model in which the absorption- and emission gas are co-spatial. They concluded that the absorbing gas is of much lower metallicity and located further away from the host galaxy than the EELR. Although they favoured the idea that the diffuse metagalactic background radiation (hereafter MBR) rather than the parent AGN was responsible for ionizing the absorbing haloes, in their calculations B00 and J03 used a simple powerlaw as a crude approximation of the MBR energy distribution. In this paper, we will assume more realistic SEDs that take into account the cumulative opacity of IGM Lyman limit systems and Ly α forest absorbers.

As for the possibility of collisional ionization of the shells, we indicated in J03 that this mechanism was unlikely in the case of 0200+015, and that steady-state photoionizing shocks (Dopita & Sutherland 1996) resulted in rather large $N_{\rm HI}$ columns ($\sim 10^{19}\,{\rm cm}^{-2}$), incompatible with the small value characterizing 0200+015. In the case of 0943–242, the near solar metallicity models of Dopita & Sutherland (1996) do not attain the observed $N_{\rm CIV}$ value for shock velocities below 400 km s⁻¹ and above this velocity the $N_{\rm HI}$ column becomes excessive, requiring the shock structure to be truncated. As for the photoionized precursor nebula upstream from the shocks, the SED generated downstream by fast shocks is as hard as a powerlaw of index $\alpha \simeq -0.5$ up to $\gtrsim 500\,{\rm eV}$ (Binette, Dopita & Tuohy 1985). Therefore, photoionization calculations with a pow-

erlaw as presented in Sect. 4.2 capture the main features of such a precursor. In essence, any hard SED requires supersolar metallicities in order to fit the column ratios found in 0200+015. Finally, calculations to represent the case of a collisionally ionized gas slab at temperature T has been explored by J03. They find that for 0200+015, the $N_{\rm CIV}/N_{\rm HI}$ column ratio could be reproduced by using roughly solar metallicities, provided that T is finetuned to lie around 10^5 K. Apart from the fact that this metallicity is rather large for the redshift considered, it would be difficult to explain how the plasma could be maintained at a temperature approaching the peak of its cooling curve. This would most likely require a yet unknown heating mechanism.

1.3. The case for a simple scattering screen

In a morphologically and kinematically complex EELR, one cannot readily disentangle photon destruction due to line-of-sight absorption from the effects of transmission by multiple scatterings. Nevertheless, for the large scale absorbing haloes in 0200+015 and 0943-242 (or other HzRGs studied by VO97), there is no evidence that the absorbers share the complexity of the EELR. The results suggest that a uniform foreground scattering screen provides an adequate description of the "absorbing" haloes in Hzrgs. Strong evidence for this was provided by observations at much higher spectral resolution using VLT-UVES (e.g. J03 and W04). In particular, J03 finds that the main absorber in 0943-242 remains as a single system of column density $\sim 10^{19}\,\mathrm{cm}^{-2}$ over the full size of the EELR, being completely black at its base, with no evidence for substructure or a multiphase environment. The absorption trough is blueshifted by $265 \,\mathrm{km}\,\mathrm{s}^{-1}$ with respect to the centroid of the background emission profile. This spatial and kinematical coherence of the absorber contrasts with the chaotic multiphase medium encountered in the Galactic ISM or the EELR of Hzrgs. It also suggests that the absorber is physically separate from the background EELR and that it is therefore simply acting as a scattering surface, as argued in J03. This clean separation between EELR and the absorber simplifies the modelling task and justifies the ionization-stratified slab approximation adopted in Sect. 4.

1.4. Comparison with the Lynx Arc Nebula: LAN

Following an independent study of the lensed Lynx Arc Nebula⁴ at z=3.357 by some of us (Fosbury et al. 2003), it was observed that the column ratios $N_{\rm CIV}/N_{\rm HI}$ in the LAN and 0200+015 are very similar. In the calculations which follow, we therefore explicitly compare the LAN and the HzRGs absorbers, making use of the following insights which place the physical conditions in the LAN on a firm footing. Firstly, the LAN is an active star-forming object,

⁴ The Lynx Arc Nebula is a high-redshift metal-poor gravitationally lensed H II galaxy that was discovered serendipitously by Holden et al. (2001).

so we may reasonably assume that the subsolar metallicity that characterizes the emission gas, $\sim 10\%$ (following the work of VM04), also applies to the absorbing gas. Secondly, the LAN presents a relatively high excitation emission line UV spectrum, which photoionization by hot stars can reproduce successfully. Photoionization by a straight powerlaw⁵, on the other hand, would result in the emission of a detectable N v λ 1240 line (comparable in strength to N IV] λ 1485 line, see BG03), which is not observed. Hence, for this object, we know the absorber metallicity and excitation source with some confidence. Therefore, the successful reproduction of the LAN column ratios in Sect. 4.4 using subsolar metallicities and photoionization by hot stars, prompts us to consider that such an SED might also apply to the HzRG absorbers.

1.5. Metallicity evolution vs. softer ionizing SED

With the VLT-UVES, J03 obtained superb spectra of the aforementioned HzRGs at ten times the resolution used by VO97. The spectra confirmed that the main absorber in 0943-242 exhibits no additional substructure to that reported by VO97, as already discussed. In contrast, a very different view of 0200+015 emerges: the single absorber with HI column density $\sim 10^{19}\,\mathrm{cm}^{-2}$ seen at low resolution now splits into two $\sim 10^{14.6}\,\mathrm{cm}^{-2}$ systems; these extend by more than 15 kpc to obscure additional Ly α emission coincident with a radio lobe. Additional but fragmented absorbers are seen on the red wing of the emission line at this position. We recall that gas metallicities as high as $\sim 10 \, Z_{\odot}$ are required to reproduce the $N_{\rm CIV}/N_{\rm HI}$ ratio in 0200+015 (Sect. 1.5; J03) assuming photoionization by a straight powerlaw. This suggests that the absorbing gas has undergone very substantial metal enrichment. Based on the smaller radio source size in 0943-242 (26 kpc versus 43 kpc for 0200+015), J03 conjectured that the radio source age (as inferred from its linear size) is the parameter controlling the evolution of: (i) the structure/kinematics of the absorbing halo, through interaction and shredding of the initially quiescent shells; and (ii) its metallicity built-up, through enrichment by starburst superwind triggered concurrently with the nuclear radio source.

Although this age and enrichment scenario (B) remains an appealing possibility, the large metallicity gap inferred by J03 of three orders of magnitude between 0943–242 ($\sim 0.01\,Z_\odot$) and 0200+015 ($\sim 10\,Z_\odot$) is a cause for concern. Here we revisit the issue by exploring alternative ionizing SEDs that would require only a factor of ten metallicity enhancement with respect to 0943–242. We focus on the case of SEDs from hot stars and the dif-

fuse MBR with the aim of generating a grid of models for comparision with future observations.

2. The observational dataset

In this section, we gather together the principal observational results which we aim to reproduce, namely the HI and CIV column densities for the absorbers in the two Hzrgs and the LAN.

The C IV and the Ly α absorption columns in 0943–242 $(z_e = 2.922)$ and 0200+015 $(z_e = 2.230)$ have been measured by various authors (Röttgering et al. 1995; B00, J03, W04). We adopt the values of J03, which are based on VLT-UVES observations of both HzRGs. In 0943-242 the dominant large scale absorber is characterized by an $N_{\rm H\,I}$ column of $10^{19.1} \,\mathrm{cm}^{-2}$, which puts it among the group of larger H I columns (see W04). However, the four Ly α absorbers observed in 0200+015 are rather thin, with columns of order $10^{14.7}\,\mathrm{cm}^{-2}$. These all belong to the group of smaller H I columns haloes, which are much more numerous (see W04). In 0943–242, the C IV $\lambda\lambda$ 1548, 1551 doublet is observed in absorption at the same redshift as the dominant H_I absorber (J03; B00; Röttgering & Miley 1997) and corresponds to a column of $10^{14.6}$ cm⁻². In the case of 0200+015, only one HI absorber, with $N_{\rm HI}=10^{14.7}\,{\rm cm^{-2}}$ shows a corresponding C IV doublet in absorption, with $N_{\rm CIV}=10^{14.6}\,{\rm cm^{-2}}$. The $N_{\rm CIV}/N_{\rm HI}$ column ratios for 0943-242 and 0200+015 are $10^{-4.5}$ and $10^{-0.07}$, respectively.

As for the LAN, the two local absorption systems in the Lynx Arc have been labelled a1 and a2 by Fosbury et al. (2003) who determined the H I column to be 1.05×10^{15} and 0.60×10^{15} cm⁻², respectively, and the C IV columns to be 0.83×10^{15} and 1.02×10^{15} cm⁻², respectively. The $N_{\rm CIV}/N_{\rm HI}$ column ratios for a1 and a2 are therefore $10^{-0.10}$ and $10^{0.23}$, respectively. The similarity of a1 with 0200+015 is noteworthy.

3. Photoionization models and ionizing energy distributions

3.1. MAPPINGS Ic and gas abundances

To compute the $N_{\rm CIV}/N_{\rm HI}$ ratio, we have used the code MAPPINGS IC (Binette, Dopita & Tuohy 1985; Ferruit et al 1997). To represent solar abundances, we adopt the set of Anders & Grevesse (1989). When varying metallicities, we multiply the solar abundances of all elements heavier than He by a constant, which we label the gas metallicity (in units of Z_{\odot}). For the HzRG absorber, we assume a slab geometry illuminated on one side. For each ionizing SED that we considered, we calculated the equilibrium ionization state of the gas and integrated the ionization structure inward until a preselected target value of the column $N_{\rm HI}$ was reached. For the range of parameters explored in this paper – where the aim is to reproduce the observed $N_{\rm HI}$ and the $N_{\rm CIV}/N_{\rm HI}$ column ratios – all models of the absorbers turn out to be matter-bounded

⁵ The possibility that the LAN corresponded to photoionization by a quasar powerlaw that is partly absorbed has been investigated by Binette et al. (2003: BG03). In order to work, such an absorbed powerlaw model requires a very specific and unlikely fine tuning of the parameters defining the EELR and the hidden filtering screen.

(0200+015) or marginally optically thick to the ionizing radiation (0943-242).

3.2. Continuum softness

For a given input SED, the calculations are repeated for different values of the ionization parameter⁶ in order to build a sequence of models in U, starting at the minimum value of 0.001.

It is customary to define the SED's softness using the parameter η , which is the column ratio of singly ionized He to neutral H, $N_{\rm HeII}/N_{\rm HI}$. This ratio does not, however, uniquely define the SED, as η also depends on the slab thickness and on U, and not just on the continuum's shape (see for instance Appendix A of Fardal et al. 1998). In the case of stellar SEDs, η varies rather abruptly with $T_{\rm eff}$. For instance, η is 1480 for a 71 000 K star while for a 80 000 K star its value is only 95. Next to each SED in Fig. 1, we indicate the value of η calculated between brackets, assuming $N_{\rm HI}=10^{14.8}\,{\rm cm}^{-2}$ and U=0.1. We now review the various SEDs displayed in Fig. 1 and used in the calculations reported in Sec. 4.

3.3. AGN powerlaw SED

In the case of direct photoionization by an AGN, we assume a simple power law of index $\alpha = -1.0$ as in B00 (with $J_{\nu} \propto \nu^{+\alpha}$). This SED is represented by the gray long-dashed line in Fig. 1a.

3.4. SED of the diffuse metagalactic radiation (MBR)

The integrated ultraviolet flux arising from distributed QSOs and/or from hot massive stars (in metal-producing young galaxies) is believed to be responsible for maintaining the intergalactic diffuse gas, the ${\rm Ly}\alpha$ forest and Lyman limit systems in a highly ionized state. The spectrum and intensity of the diffuse MBR is affected not only by photoelectric absorption from intergalactic matter, but also by the re-emission from radiative recombinations within the absorbing gas itself. In short, QSO absorption-line systems are sources, not just sinks of ionizing photons, as shown by Haardt & Madau (1996).

Detailed calculations of the propagation of QSO and stellar ionizing radiation through the intergalactic space have been presented by Fardal et al. (1998; FGS in the figures or footnotes) and the resultant SEDs relevant to the current work⁷ are shown in Fig. 1a. On the one hand, we have the metagalactic SED in which *only* quasars are

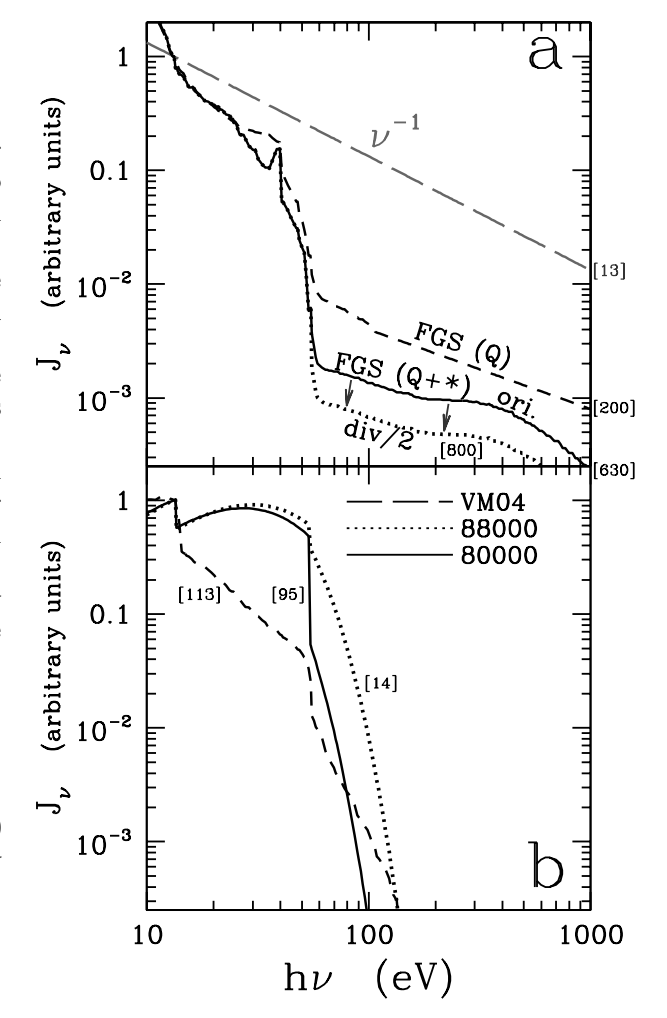


Fig. 1. The spectral energy distribution of various ionizing sources (see Sect. 3) as a function of photon energy. Panel a: silver long-dashed line: spectral energy distribution corresponding to an AGN powerlaw, short dashedline: diffuse MBR energy distribution from FGS at $z_{\rm a}=2$ comprising only quasars (Q) as sources, continuous line: (original) MBR energy distribution from FGS at $z_a = 3$ comprising both quasar and stellar sources $(Q+\star)$, dotted line: same as solid line except that the flux beyond 54.4 eV has been reduced by a factor two. Panel b: continuous line: SED of a zero-age metal-free star of effective temperature 80 000 K, dotted-line: SED of a zero-age metal-free star of effective temperature 88 000 K, long-dashed line: SED from an evolutionary model of CMK04 corresponding to an age of 3.4 Myr and metallicity of 20% solar. Values of η are given between brackets for each SED (Sec. 3.2).

contributing (short dashed line) corresponding to model Q2 in their Fig. 7 and, on the other, the SED in which hot stars from star forming regions are included (continuous line), a model shown in their Fig. 6. In this model, the stars are contributing twice the flux of quasars at 13.6 eV. The dotted line is a similar SED, except that the flux be-

⁶ We use the customary definition of the ionization parameter $U = \varphi_{\rm H}/cn_{\rm H}$ as the ratio between the density of ionizing photons impinging on the slab $\varphi_{\rm H}/c$ and the total H density at the face of the slab $n_{\rm H}$.

⁷ The SEDs calculated by FGS are softer than those of Haardt & Madau (1996). In their Appendix A, FGS justifies this difference on account of a more detailed treatment of the cloud opacity and re-emission.

yond 4 Ry has been divided by two. It is an adhoc model representing the case in which stars are contributing proportionally more with respect to quasars (a similar SED was also considered by Telfer et al. 2002).

The sharp drop of flux at 54.4 eV is a characteristic of all metagalactic radiation models and is due to the cumulative opacity of He II within the IGM. As the IGM SEDs extend into the soft X-rays, it is important to include the harder radiation beyond $\gtrsim 200\,\mathrm{eV}$, otherwise the calculated C IV columns are affected, especially when U is large.

If we turn to the values of the softness parameter (Sect. 3.2) observed among IGM absorbers, there is a substantial dispersion in the values measured by Kriss et al. (2001), with $1 \lesssim \eta \lesssim 1000$, which suggests that for a fraction of absorbers, stellar ionizing sources might be contributing. The possibility of a rather inhomogeneous distribution of the SED hardness according to location is favoured by the independent study of Smette et al. (2002), who find that $20 \lesssim \eta \lesssim 5000$.

3.5. Stellar ionizing SEDS

In the stellar ionizing case (panel b in in Fig. 1), we considered metal-free stellar SEDs that approximate those studied by Schaerer (2002) with $T_{\rm eff}$ among one of the following values: $42\,000$, $57\,000$, $71\,000$, $80\,000$ and $88\,000\,\mathrm{K}$. In Fig. 1b, we illustrate the cases of the 80 000 and 88 000 K SEDs (the continuous and dotted lines, respectively). As in BG03, who presented various photoionization models for the LAN, we approximate the selected stellar SEDs, using a technique that reproduces the ionizing photon luminosities Q(H), $Q(He^0)$ and $Q(He^+)$ of the selected $\log T_{\rm eff}$ model listed in Table 3 of Schaerer (2002). In a similar fashion to Shields & Searle (1978), we derive the monochromatic temperatures at the edge boundaries $T_{\rm H^0}^+$, $T_{\rm He^+}^-$ and $T_{\rm He^+}^+$, and then interpolate linearly in log T_{ν} for all the wavelengths used in the code MAPPINGS Ic. We equated $T_{\rm H^0}^-$ to $T_{\rm eff}$ and neglected the very small ${\rm He^0}$ edge present in these atmospheres. This simplified representation of a stellar atmosphere provides enough accuracy to compute the essential properties of the emission line spectrum.

We additionally considered an SED derived from the stellar evolutionary model of Cerviño, Mas-Hesse & Kunth (2004, hereafter CMK04), which was used by Villar-Martín et al. (2004; VM04) in their photoionization calculations of the LAN. The selected SED corresponds to a metallicity $Z_* = 0.20\,Z_\odot$ and an age of 3.4 Myr. It is represented by the long-dashed line in Fig. 1b. We included the weak X-ray flux that results from the conversion of the kinetic energy of the supernova remnants into X-ray emission (it did not have any effect on the results). The stellar cluster at that particular age harbours an important population of WR stars and, as shown by VM04, the resulting ionizing continuum is sufficiently hard to reproduce the emission line strength of the He II λ 1640 line observed in

the LAN spectrum. The CMK04 evolutionary models are characterized by a powerlaw initial mass function with a Salpeter IMF and stellar masses comprised in the range $2\text{--}120\,\mathrm{M}_{\odot}$.

4. Model results

In this section, we present a grid of photoionization calculations for comparison with the observed $N_{\rm CIV}/N_{\rm HI}$ ratios in the two Hzrgs and the Lan. In Sect. 4.1, we outline our investigative procedure and the format we adopt to display the results. Thereafter, we explore the effects of using different SEDs and varying some of the input parameters, as follows: (a) powerlaw photoionization is first studied in Sect. 4.2 assuming different metallicities; (b) in Sect. 4.3 we study various MBR energy distributions in which quasars and stars are contributing in different proportions; (c) in Sect. 4.4 we explore stellar photoionization by metal-free atmospheres of varying $T_{\rm eff}$ and by a stellar cluster SED containing WR stars.

4.1. Aims and modelling procedure

There is a gap of more than four orders of magnitude in the $N_{\rm CIV}/N_{\rm HI}$ ratio between 0943–242 and 0200+015. Rather than explain this with a factor ~ 1000 difference in absorber metallicity between the two Hzrgs as in J03, we instead explore alternative SEDs. As stated in Sec. 1.5, our practical goal is to find an SED which reduces the metallicity gap to ~ 10 (that is, obtaining a successful model that use abundances as low as $\sim 10\%$ solar). We do not aim at obtaining exact fits of this ratio in each case, but rather at establishing an order of magnitude agreement between the models and the separate observations of the thin and thick absorber categories. For this reason, we only consider the following four widely spaced metallicities for the haloes: 10, 1, 0.1 and 0.01 Z_{\odot} . The higher the metallicity, the larger the $N_{\rm CIV}/N_{\rm HI}$ ratio. The proportionality is linear except in the high metallicity regime, where the slab temperature structure is somewhat altered, this effect being more important in the case of the thick absorbers. No attempt is made in this paper to model the background EELR spectrum. The metallicity of the EELR gas is much higher than (and unrelated to) the absorber's, as discussed by B00.

The ionization parameter characterizing the models is plotted on the abscissa in all figures. It is a free parameter that cannot be adequately constrained with the limited data at hand. The target $N_{\rm CIV}/N_{\rm HI}$ ratio (y-axis) for each observational datum is represented by an horizontal (thick broken) line, since U is not known. Our aim will be to find models that either cross this observational line or come close to it. We consider it unlikely that U is smaller than 0.001, since C^{+3} would then be reduced to a trace species. It is plausible that it takes on much larger values instead, especially in the case of 0200+015 or the LAN, since large values of U usually result in larger $N_{\rm CIV}/N_{\rm HI}$ ratios, a characteristic of these thinner absorbers. We adopt the

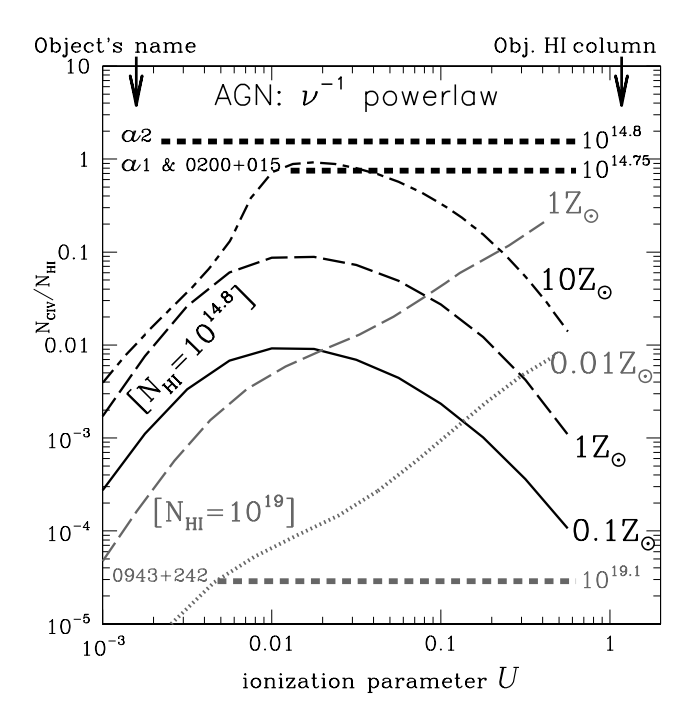


Fig. 2. The column ratio $N_{\rm CIV}/N_{\rm HI}$ derived from photoionization by a powerlaw of index -1.0, as a function of the ionization parameter U. Each model sequence (thin lines) along which U varies represents a slab of fixed $N_{\rm HI}$ column (shown between brackets). Thin black lines connect models of constant column $N_{\rm HI} = 10^{14.8} \, \rm cm^{-2}$, while thin gray lines connect models of constant column $N_{\rm HI} = 10^{19} \, {\rm cm}^{-2}$. The gas metallicity is shown using labels, in units of Z_{\odot} . The thick horizontal broken lines represent four measurements of $N_{\rm CIV}/N_{\rm HI}$: the extended absorbers in the high-z radio galaxies 0943–242 (in gray) and 0200+015 (in black) and the two absorbers found in the lensed Lynx Arc Nebula [LAN] (in black) and labelled a1 and a2 by Fosbury et al. (2003). The ratios for 0200+015and a1 are very similar and have been combined into a single entry. The object's name and the $N_{\rm HI}$ column appear to the left and right, respectively, of the corresponding horizontal broken line.

conservative view that most of the difference between the thin and thick absorbers may be accounted for by differences in the gas excitation, that is, in U rather than by metallicity differences only. Future observations of other resonance lines might be used to test this (see Sec. 6.1).

In what follows, the slab models presented are either characterized by a small H I column of $10^{14.8}$ cm⁻² as in 0200+015 and the LAN, or a larger column of 10^{19} cm⁻² as in 0943-242. We emphasize that in all the figures (2–6) of Section 4, the black line models only apply to the thin absorbers shown at the top while the gray-line models only apply to 0943-242 (shown at the bottom).

4.2. Powerlaw photoionization

We present photoionization calculations in Fig. 2 for the case of an AGN powerlaw of index -1.0. Using a mod-

erately different index would not significantly alter the conclusions reached below. For instance, a steeper index -1.4 would increase the column ratio only by a factor of $\lesssim 2$.

In the case of the 0943–242 absorber, the models in Fig. 2 (thin gray lines) favour abundances much lower than solar, that is of order 1% solar. B00 favoured a metallicity value of $\simeq 0.02\,Z_{\odot}$. A much lower (higher) ionization parameter is a possibility that cannot be ruled out and the metallicity would then be higher (lower) than the values we considered.

In the case of the 0200+015 absorber, very high metallicities are favoured by the powerlaw SED, as found by J03. This is shown by the thin black lines in Fig. 2, which suggest a gas metallicity of about ten times solar. We expressed concerns about such high values in Sect. 1.5.

We reject the powerlaw SED on account of geometrical considerations presented in Sect. 1.2 that led us to rule out direct ionization by the nuclear radiation from the AGN. The main purpose in reporting powerlaw calculations is to provide a convenient comparison with the softer continuum shapes explored below. We note how different the behaviour of $N_{\rm CIV}/N_{\rm HI}$ is between the thin and thick absorber case in Fig. 2 (compare the two long-dashed models of solar metallicity).

4.3. Photoionization by the diffuse MBR

4.3.1. MBR flux from quasars alone

The SED of the diffuse MBR resulting from quasars alone (black long-dashed line in Fig. 1a) is significantly softer than a powerlaw. Calculations with such an SED are shown in Fig. 3. The calculated $N_{\rm CIV}/N_{\rm HI}$ ratio assuming 10% solar gas lies below the observed value in 0200+015, by a factor ~ 10 , as shown by the continuous thin line model in Fig. 3. Metallicities about solar would be required so that the model overlaps the observed column ratio⁸. As for 0943–242, in absence of definite information about U, the absorber's metallicity cannot be constrained any further than in the previous powerlaw case covered in Sect. 4.2.

4.3.2. MBR flux from stars and guasars

In the case in which stars and not just quasars contribute to the MBR, the ionizing SED becomes softer (continuous line in Fig. 1a) and the $N_{\rm CIV}/N_{\rm HI}$ ratio observed in 0200+015 can now be reproduced using metallicities not much above 10% solar, as illustrated by the thin dashed line in Fig. 4. The short-long dashed thin line in Fig. 4 represents the case of an even softer SED in which the flux beyond 54 eV has been halved (see dotted line SED in Fig. 1a). This latter SED hence satisfies our initial goal defined in Sect. 4.1 with respect to metallicity. But adopt-

⁸ Hence in the thin slab case, the increase in $N_{\rm CIV}/N_{\rm HI}$ provided by a quasar-based MBR SED is a factor ten with respect to a straight AGN powerlaw.

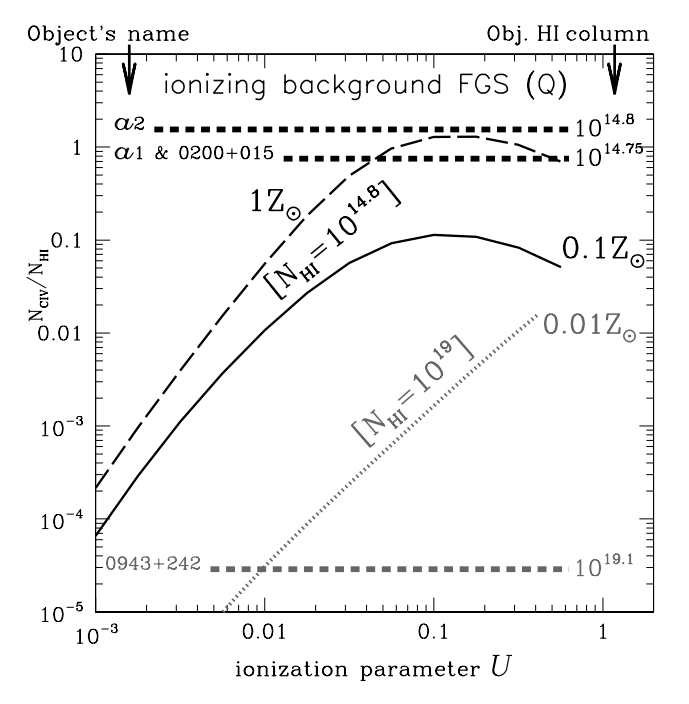


Fig. 3. The column ratio $N_{\rm CIV}/N_{\rm HI}$ derived from photoionization by the diffuse MBR due to quasars only, as a function of U. The continuous black line and the long-dashed black line correspond to the thin absorber case assuming metallicities of 0.1 solar and solar, respectively, while the dotted gray line corresponds to the thick absorber case assuming metallicities of 0.01 solar. The nomenclature and symbols have the same meaning as in Fig. 2. In all figures, black line models only apply to the thin absorber objects shown at the top, while gray-line models only apply to 0943–242 below.

ing an SED in which star-forming galaxies are contributing more than quasars does not imply that such a distribution is typical of the average MBR. It only suggests that this SED is valid in the neighborhood of 0200+015. Smette et al. (2002) found for instance that the softness of the MBR energy distribution (parameter η , see Sect. 3.2) presents important local variations, with some locations where only quasars are apparently contributing while in others there appears to be a significant contribution from starbursting galaxies.

In the case of the thicker absorber in 0943–242, there is little difference in $N_{\rm CIV}/N_{\rm HI}$ between the Q+ \star SED in which the flux beyond 54 eV has been halved and the SED produced by quasars only. Compare, for instance, the gray dotted lines $(0.01\,Z_{\odot})$ in Figs 3 and 4.

In summary, a diffuse MBR sustained by quasars and star-forming galaxies is quite successful in reproducing the observed column ratio in 0200+015 without need for a metallicity any higher than $\sim 0.10\,Z_{\odot}$.

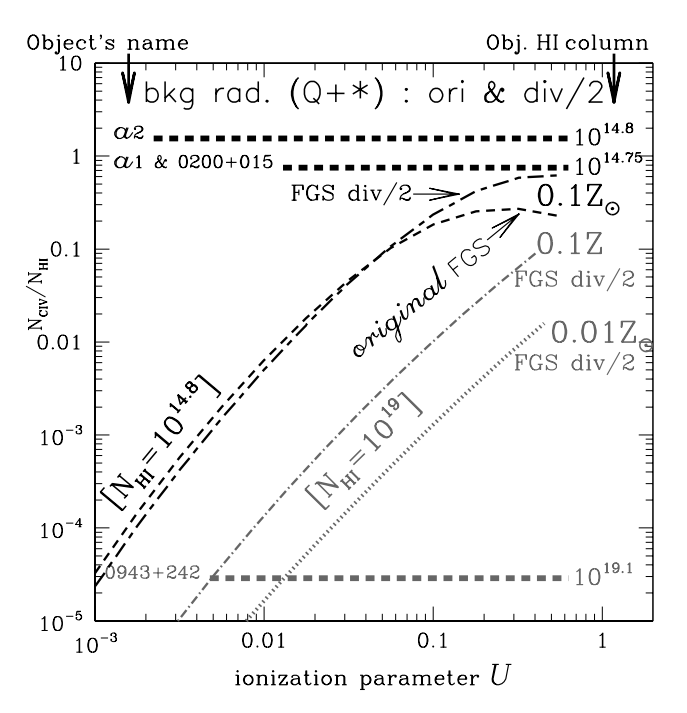


Fig. 4. The column ratio $N_{\rm CIV}/N_{\rm HI}$ derived from photoionization by the MBR due to stars and quasars, as a function of U. The black short-dashed line corresponds to photoionization by the original FGS SED in which the MBR flux is generated by quasars as well as stars, assuming a gas metallicity of $0.10\,Z_{\odot}$. The black short-long dashed line has an SED similar to the previous, but its flux beyond 54 eV has been halved (the dotted-line SED in Fig. 1a), owing to a larger contribution by stars. The gray dot-dashed line and gray dotted line assume this latter SED in the thick slab case, but with metallicities of 0.1 and $0.01\,Z_{\odot}$, respectively. The nomenclature and symbols have the same meaning as in Fig. 2.

4.4. Photoionization by local stellar UV

4.4.1. Photoionization by hot stars with $T_{\rm eff}$ =80 000 K

Using a metal-free stellar atmosphere of 80 000 K and a gas metallicity of 4% solar, BG03 obtained a reasonable first order fit to the strong lines observed in the unusual spectrum of the high redshift LAN. In Fig. 5, we show that the column density ratios of the LAN absorbers can be reproduced using a high value of U and an absorption gas metallicity of $0.1-0.2 Z_{\odot}$. This range is consistent with the comprehensive metallicity determination of the nebular emission gas by VM04, that is $\simeq 10\%$ solar. Given the similarity of the LAN column ratio with that of 0200+015, we infer that a $N_{\rm CIV}/N_{\rm HI}$ ratio of order unity in an HzRG is compatible with a stellar SED photoionizing a subsolar metallicity absorber. Hence, the possibility that the 0200+015 absorber might be photoionized by hot stars warrants consideration, since metallicities of only 10% solar would be needed rather than a value 100 times larger favoured by the powerlaw SED (Fig. 2 or J03). The problem of stellar continuum detection is discussed in Sect. 5.2.2.

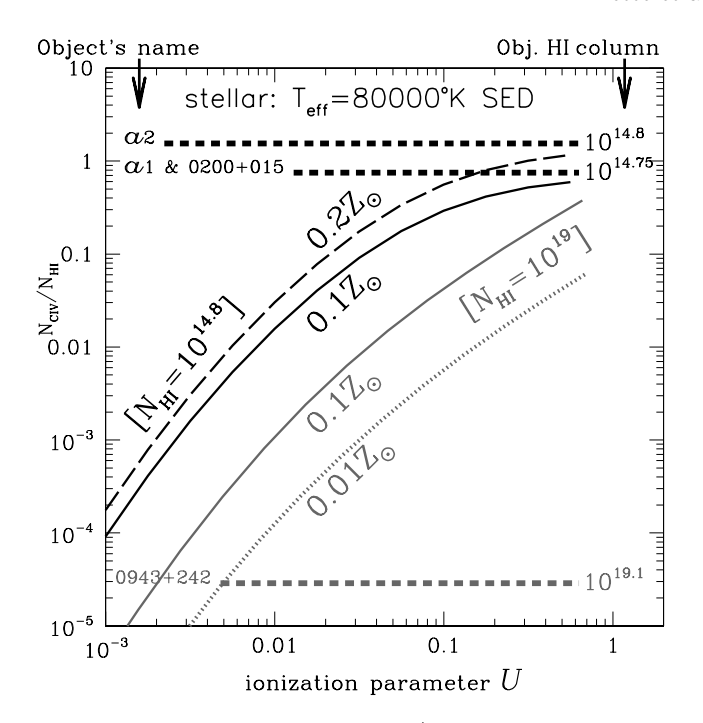


Fig. 5. The column ratio $N_{\rm CIV}/N_{\rm HI}$ derived from photoionization by a metal-free stellar atmosphere with $T_{\rm eff}{=}80\,000\,{\rm K}$ as described in Sect. 3.5, as a function of U. The nomenclature and symbols have the same meaning as in Fig. 2.

In the case of thicker absorbers, as represented by 0943–242, the gray line models point to metallicities in the range 0.01–0.1 Z_{\odot} , assuming U < 0.05. Higher values of U would imply lower absorber metallicities. Interestingly, the stellar (Fig. 5) and the powerlaw (Fig. 2) models with 0.01 Z_{\odot} cross the $N_{\rm CIV}/N_{\rm HI}$ ratio of 0943–242 at a very similar U value. This indicates that thicker slabs are much less sensitive to the SED's shape.

4.4.2. Varying the stellar atmosphere temperature

In Fig. 6 we explore the effect of varying stellar effective temperature. The zero-age metal-free atmospheres used correspond to $T_{\rm eff}$ of 42 000, 57 000, 71 000, 80 000 and $88\,000\,\mathrm{K}$ (from Schaerer 2002). All models are characterized by a column $N_{\rm HI} = 10^{14.8} \, {\rm cm}^{-2}$ and a gas metallicity of 10% solar, appropriate to the LAN. Although temperatures lower than 80 000 K can easily fit the LAN column ratio, this would imply too weak He II $\lambda 4686$ emission for the nebula. At the other temperature end, a $T_{\rm eff}$ as high as 88 000 K would require a ten times higher gas metallicity in order to reproduce the observed column ratio. The reason is that, as $T_{\rm eff}$ is increased much beyond 70 000 K, the increase in the continuum's hardness causes the slab to harbour many ionization stages of carbon (e.g. C⁺⁴ and C^{+5}), thereby causing a relative reduction of the C IV fraction. Increasing the temperature much beyond 10⁵ K would result in column ratios approaching those of a powerlaw.

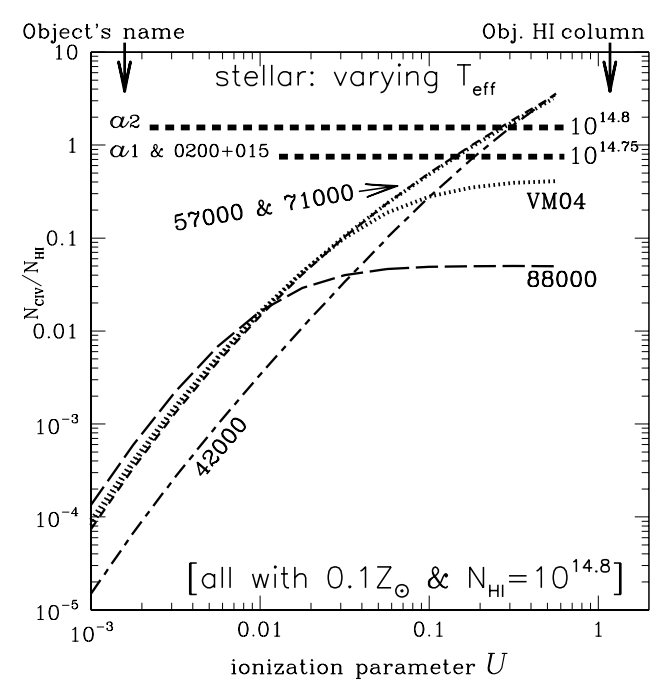


Fig. 6. The column ratio $N_{\rm CIV}/N_{\rm HI}$ derived from photoionization by stellar energy distributions of varying $T_{\rm eff}$, as a function of U. In all models, the metallicity is $0.1\,Z_{\odot}$ and the slab opacity $10^{14.8}\,{\rm cm}^{-2}$. A label shows the $T_{\rm eff}$ being considered. The dotted line labelled VM04 corresponds to photoionization by a stellar cluster of metallicity 20% solar and 3.4 Myr of age, as described in Sect. 3.5. The nomenclature and symbols have the same meaning as in Fig. 2.

VM04 have modelled the LAN emission line spectrum using the ionizing spectrum of an evolved stellar cluster in which transient Wolf-Rayet stars can account for the nebular He II $\lambda 4686$ line observed in emission. A photoionization model of the absorber using such an SED is represented by the dotted line labelled VM04 in Fig. 6. The behaviour of the column ratio is similar to that of a 80 000 K metal-free star (Fig. 5).

In the case of the HZRG shells, stellar SEDs are possible candidates for the ionization of the absorbers (but not of their EELR), since they can reproduce the observed column ratio using subsolar metallicities.

5. Estimates of the radii and masses of the shells and compatibility with other observables

Armed with the results of the photoionization calculations, we now investigate two of the scenarios in more detail, namely the cases of ionization by the MBR and by hot stars. We focus on their implications for other properties of the absorbing shells (e.g. mass, radius and thickness) and their compatibility with other observables (e.g. the underlying stellar continuum in the case of ionization by hot stars, and the strength of the $\text{Ly}\alpha$ emission). On the basis of such considerations we demonstrate that ionization by hot stars is favoured over MBR ionization. Readers

who do not wish to follow the argument in full may skip over sections 5.1 and 5.2 and proceed directly to the summary in section 5.3.

5.1. The case of MBR ionization

We first analyse the possibility of having the MBR ionize the haloes. The diffuse MBR is ubiquitous and its intensity independent of distance to the HzRG. Therefore, changes in excitation (i.e. U) are obtained by varying the gas density. Higher shell densities, hence lower U, might explain the absence of C IV absorption in many HzRG shells. We must thus investigate whether the MBR is strong enough to result in an acceptable halo density, because the geometrical thickness of the shell increases as the density is reduced. Below we use such constraints to infer the shell's minimum distance from the HzRG and its total mass.

5.1.1. MBR intensity and shell thickness

An estimate of the MBR mean intensity is provided by the proximity effect, whereby absorbers becoming more ionized in the vicinity of quasars. We will adopt the value $J_{\nu} \approx 10^{-21} \,\mathrm{erg}\,\mathrm{cm}^{-2}\,\mathrm{s}^{-1}\,\mathrm{Hz}^{-1}\,\mathrm{sr}^{-1}$ inferred by Cooke, Espey & Carswell (1997) and assume the MBR flux SED $Q+\star$ of Fardal et al. (1998), albeit with the flux above 4 Ry divided by two, as studied in Sect. 4.3.2. We will consider two cases: the weak and the strong absorber cases, using 0200+015 and 0943-242 as examples, respectively. Using the definition of U and MAPPINGS IC to integrate the $Q+\star$ SED, we obtain in the optically thin case that the total hydrogen density is given by $n_{\rm H}^{\rm thin} = 2.8 \times 10^{-4} J_{-21} \{ U_{0.1}^{\rm thin} \}^{-1} {\rm cm}^{-3}$, where $U_{0.1}^{\rm thin} = U^{\rm thin}/0.1$ and $J_{-21} = J_{\nu}/(10^{-21} {\rm erg \, cm}^{-2} {\rm s}^{-1} {\rm Hz}^{-1} {\rm sr}^{-1})$. In the case of thicker absorbers with $N_{\rm H} \gtrsim 10^{18}\,{\rm cm}^{-2}$, because of self-shielding, illumination of a spherical shell can only occur from the outside, and the mean intensity is approximately half of the previous thin case, such that $n_{\rm H}^{\rm thick}=2.8\times10^{-3}J_{-21}\{U_{0.005}^{\rm thick}\}^{-1}{\rm cm}^{-3}$, where (for convenience) $U_{0.005}^{\rm thick}=U^{\rm thick}/0.005$. The photoionization calculations at constant $N_{\rm HI}$ (either $10^{14.8}$ or 10^{19} cm $^{-2}$) indicate that the total hydrogen column of the slab can be approximated as $N_{
m H}^{
m thin} \simeq 2.1 \times 10^{19} \, \{U_{0.1}^{
m thin}\}^{1.1} \, {
m cm}^{-2}$ and $N_{
m H}^{
m thick} \simeq 6.3 \times 10^{20} \, \{U_{0.005}^{
m thick}\}^{1.1} \, {
m cm}^{-2}$, respectively. As argued in Sect. 1.3, a shell geometry is more appropriate than that of a filled sphere. We therefore introduce an aspect ratio $A = \Delta r/r$ for the shell, where Δr is the shell thickness and r its outer radius, taking the HzRG nucleus as the center. Since this ratio is not known, we will define an upper limit of $A \lesssim 0.2$. Since the total column density is given by $N_{\rm H} = r n_{\rm H} A$, this limit on A translates into a lower limit for the shell radius (i.e. a minimum radius) of $r_{\rm kpc}^{\rm thin} \geq 122 \{U_{0.1}^{\rm thin}\}^{2.1} \{A_{0.2}J_{-21}\}^{-1} \,{\rm kpc}$ and $r_{\rm kpc}^{\rm thick} \geq 365 \{U_{0.005}^{\rm thick}\}^{2.1} \{A_{0.2}J_{-21}\}^{-1} \,{\rm kpc}$, respectively, with $A_{0.2} = A/0.2$. To be definite, we will assume that both absorbers have the same gas metallicity of $0.10 \, Z_{\odot}$. From Fig. 4, we read off values of $U_{0.1}^{\rm think} \simeq 2$ and $U_{0.005}^{\rm think} \simeq 1$ for 0200+015 and 0943-242, respectively. This translates into minimum radii of 523 and 365 kpc, respectively. Hence MBR ionization implies that the shells are extremely distant from the background EELR, and this appears to be difficult to reconcile with the observations which show a distinct transition from sources with radio extents < 25 kpc to those with large radio sizes (see section 5.2.1).

Since $r_{\rm kpc} \propto U^{2.1}$, smaller radii follow from assuming smaller values of U, which would require that we adopt metallicities somewhat larger than $0.1\,Z_{\odot}$ (larger metallicities shift models to the left in Fig. 4). Uncertainties in U (or equivalently in Z) therefore affect our estimates of the shell's geometrical thickness significantly. In Sect. 6.1 and 6.2, we indicate how detection of the shells in Mg II or O VI would help to constrain both Z and U.

5.1.2. Problem of the large shell masses

Since the shell masses are given by $M_{\rm H} = 4\pi r^2 m_{\rm H} N_{\rm H} =$ $10^{-13} \, r_{\rm kpc}^2 N_{\rm H} \, {\rm M}_{\odot}$, assuming they are spherical, we can use the previous expressions for the minimum radii to derive the following minimum masses $M_{\rm H}^{\rm thin} \geq 3.1 \times$ $10^{10} \{U_{0.1}^{\rm thin}\}^{5.3} \{A_{0.2}J_{-21}\}^{-2} {\rm M}_{\odot} \text{ and } M_{\rm H}^{\rm thick} \geq 8.3 \times 10^{12} \{U_{0.005}^{\rm thick}\}^{5.3} \{A_{0.2}J_{-21}\}^{-2} {\rm M}_{\odot}, \text{ respectively. Adopting the same estimates of } U \text{ as above, we derive masses of the same estimates of } V \text{ as above, we derive masses of the same estimates of } V \text{ as a bove, we derive masses of the same estimates of } V \text{ as a bove, we derive masses of the same estimates of } V \text{ as a bove, we derive masses of } V \text{ as a bove, } V \text{ as a bove, } V \text{ and } V \text{ and } V \text{ and } V \text{ as a bove, } V \text{ and } V \text{ and } V \text{ and } V \text{ as a bove, } V \text{ and } V \text$ $M_{\rm H}^{\rm thin} \ge 1.2 \times 10^{12} \,{\rm M}_{\odot}$ and $M_{\rm H}^{\rm thick} \ge 8.3 \times 10^{12} \,{\rm M}_{\odot}$ for 0200+015 and 0943-242, respectively. At face values, these values are excessive and would suggest that MBR ionization is unworkable. On the other hand, given the strong dependence of $M_{\rm H}$ above on poorly determined quantities, the upper limits mentioned above are order of magnitude estimates and as such do not allow us to completely rule out MBR ionization. For instance, reducing both ionization parameters by two reduces the 0200+015 and 0943-242 shell mass estimates to 3.1×10^{10} and $2.1 \times 10^{11} \,\mathrm{M}_{\odot}$, respectively. Proportionally smaller masses would be implied if the shells covered only a fraction of 4π sr. On the other hand, if the shells were to be geometrically very thin (i.e. $A_{0.2} \ll 0.2$), the mass of the 0943–242 shell would become unreasonably large (> $10^{13} \,\mathrm{M}_{\odot}$).

In conclusion, the ionization of the shells by the diffuse MBR would imply that the shells have expanded to large distances from the parent Hzrg. This would favor the 'aging shell' scenario B. A significant problem is that the shell mass estimates turn out too large. An alternative is that the ionizing radiation is stronger as a result of *local* stellar sources, as discussed below.

5.2. The case of ionization by local stellar sources

The similarity of the $N_{\rm CIV}/N_{\rm HI}$ ratio between the stellar-excited LAN nebula and the 0200+015 absorber suggests that hot stars could be the ionization source of the HzRGs

⁹ If the SED was a powerlaw of index α (< 0), we would have $U \approx -4\pi J_{\nu}/(n_{\rm H}hc\alpha) = 6.3\,10^{-5}J_{-21}/n_{\rm H}$, where h is the Planck constant and c the speed of light.

haloes. Even though the emission-line spectra of the background EELR is clearly AGN-like and presumably ionized by the hidden quasar, an interesting result of the calculations in Sect. 4.4 is that the column ratios in the two HzRG absorbers can be reproduced using a stellar SED and subsolar metallicites, as for the LAN. We now analyse some of the implications of this hypothesis.

5.2.1. Test case: hot stars contributing little to the EELR

The geometry that we envisage is that of a large population of hot stars, possibly distributed uniformly or in large aggregates as a result of merging (e.g. the HzRG 4C41.17; van Breugel et al. 1997). To simplify the treatment of the geometrical dilution of the ionizing radiation, we will assume that the propagation of the photons is approximately radial by the time they reach the intervening shells. To facilitate the comparison with the previous MBR ionization case, we define a reference test case with a much higher shell density of $0.01\,\mathrm{cm}^{-3}$. The photon density is set by the relation $n_{\rm H} = 10^{-2} \{U_{0.1}\}^{-1} {\rm cm}^{-3}$, which is equivalent to having an ionizing flux (reaching the shell) 36 times higher than that provided by the MBR intensity with $J_{-21} = 1$, as assumed in Sect. 5.1.1. Under the conditions of this test case, our calculations indicate that the ionizing photon flux impinging upon the inner boundary of the shells is $\varphi_{\rm H} = 3.0 \times 10^7 \, n_{0.01} U_{0.1} \, {\rm quanta \, cm^{-2} \, s^{-1}}$, where $n_{0.01} = n_{\rm H}/0.01$ represents the shell density. Local stellar sources (in contrast to the MBR case) are in better accord with the 'inner shell' scenario A, in which the shells do not extend further out than about 25 kpc in radius, i.e. the apparent crossover point between sources with absorbers and those without [see J03; W04; Sect. 1.1 and the superwind-bowshock model of Krause (2005)]. The photon luminosity is $4\pi r^2 \varphi_{\rm H}$, which can be written as $Q_{\rm H} =$ $0.224\,10^{55}\,r_{25}^2\,n_{0.01}\,U_{0.1}\,\mathrm{quanta}\,s^{-1}$, where $r_{25}=r_{\mathrm{kpc}}/25$. The Lylpha luminosity from recombination alone is given by the expression $L_{\rm Ly\alpha} = 1.06 \times 10^{-11} \epsilon_{\rm neb} Q_{\rm H} \, \rm erg \, s^{-1}$, where the conversion factor¹⁰ assumes case B and a temperature of 20 000 K. $\epsilon_{\rm neb}$ is the fraction of photons absorbed and reprocessed by the emission gas. The leaking fraction $1-\epsilon_{\rm neb}$ for very luminous H_{II} regions lies in the range 0.3–0.5 (Beckman et al. 2000 and references therein; Zurita et. al. 2002; Relaño et al. 2002; Giamanco et al. 2005). To be definite, we adopt 0.5 and define $\epsilon_{0.5}^{\rm neb} = \epsilon_{\rm neb}/0.5$ to obtain

$$L_{\rm Ly\alpha} = 0.12 \times 10^{44} \, \epsilon_{0.5}^{\rm neb} \, r_{25}^2 \, n_{0.01} \, U_{0.1} \, {\rm erg \, s^{-1}}$$
 (1)

for our test case.

The $L_{{\rm Ly}\alpha}$ luminosity in the test case should be compared with the significantly larger EELR $L_{{\rm Ly}\alpha}$ luminosities of 1.2×10^{44} and $1.9 \times 10^{44} {\rm erg \, s^{-1}}$, observed in 0200+015 and 0943-242, respectively. In the case of the

LAN, with $L_{\rm Ly\alpha}=0.40\times10^{44}\,{\rm erg\,s^{-1}}$, its luminosity ¹¹ is three times higher than our test case. As for our two EELRs, they are brighter in Ly α by a factor 5 (0200+015) and 300 (0943–242), assuming in Eqn. 1 that $U_{0.1}^{\rm thin}\simeq2$ and $U_{0.005}^{\rm thick}\simeq1$, respectively. The assumed stellar ionizing luminosity is therefore not expected to alter the AGN character of the HzRG emission spectrum, even though specific emission lines would be subject to a contribution from the proposed stellar sources.

Interestingly, the Ly α luminosities of the absorption shells themselves are expected to be relatively small. We derive Ly α luminosities of $L_{\rm Ly}\alpha=5.5\times 10^{43}\,\epsilon_{\rm shell}\,n_{0.01}\,U_{0.1}{\rm erg\,s^{-1}}$, where $\epsilon_{\rm shell}$ is the fraction of ionizing photons absorbed by the shell, a quantity that is set by the shell opacity. Our calculations with $N_{\rm HI}$ of $10^{14.8}$ and $10^{19}\,{\rm cm^{-2}}$ indicate that $\epsilon_{\rm shell}=5\times 10^{-4}$ and 0.97 for the thin and thick absorbers, respectively. Assuming as in Sect. 5.1.1 that $U_{0.1}^{\rm thin}\simeq 2$ and $U_{0.005}^{\rm thick}\simeq 1$ for 0200+015 and 0943-242, respectively, this translates into luminosities of 5.5×10^{40} and $2.7\times 10^{41}\,{\rm erg\,s^{-1}}$, respectively. These values are negligible with respect to the observed HzRG and LAN Ly α luminosities.

As for the masses of the shells, the total column densities as a function of U in the case of stellar SED are as follows: $N_{\rm H}^{\rm thin} \simeq 1.1 \times 10^{19} \, \{U_{0.1}^{\rm thin}\}^{1.1} \, {\rm cm}^{-2}$ and $N_{\rm H}^{\rm thick} \simeq 7.2 \times 10^{20} \, \{U_{0.005}^{\rm thick}\}^{1.1} \, {\rm cm}^{-2}$, assuming the 80 000 K sed. We used the expression $M_{\rm H}=6.25\times10^{-11}\,r_{25}^2N_{\rm H}\,{\rm M}_{\odot}$, assuming again that the shells are spherical, to derive mass estimates of $M_{\rm H}^{\rm thin}=6.7\times10^8\,r_{25}^2\,\{U_{0.1}^{\rm thin}\}^{1.1}\,{\rm M}_{\odot}$ and $M_{\rm H}^{\rm thick}=4.5\times10^{10}\,r_{25}^2\,\{U_{0.005}^{\rm thick}\}^{1.1}\,{\rm M}_{\odot}$ for 0200+015 and 0943–242, respectively. Hence, the shell masses for the test case are quite small in comparison with the MBR case because of the smaller radii implied by the stronger ionizing flux. By the same token, larger densities are implied, which result in shells that are also geometrically very thin $(A_{0.2} \ll 1)$. The absorber's density can be quite different than the assumed test case with $n_{0.01} = 1$. The required stellar luminosity, however, must then scale in the same proportion. For instance, an absorber with density 0.1 cm⁻³ would require a 10 times higher stellar luminosity. This would cause the nebular lines to be comparable

Under the quoted physical conditions, 65% of the recombinations lead to Ly α photon emission (e.g. Binette et al. 1993).

¹¹ The observed $L_{\rm Ly\alpha}$ values quoted above were derived using the Ly α fluxes reported by VO97 and that of Fosbury et al. (2003) for the LAN. We assumed the objects to be isotropic emitters and corrected the fluxes for ${\rm Ly}\alpha$ absorption due to the absorbing shells. For the LAN, $L_{\rm Ly\alpha}$ was divided by 10 to compensate for the amplification by the gravitational lens. We adopted the concordance Λ CDM cosmology with parameters with $\Omega_{\Lambda} = 0.7$, $\Omega_{M} = 0.3$, h = 0.70 with $h = H_{0}/100$. The isotropic photon luminosities that we infer for 0200+015, 0943-242 and the LAN are $Q_{\rm H}=1.1\times 10^{55},\,1.8\times 10^{55}$ and 0.37×10^{55} quanta s^{-1} , respectively. These values are lower limits, since they only represent the fraction absorbed by the gas and reprocessed into line emission. To recover the intrinsic $Q_{\rm H}$, they would have to be increased by $\epsilon_{\rm neb}^{-1}$, a poorly determined quantity in AGN ($\epsilon_{\rm neb}^{\rm AGN}\lesssim 0.1$: Oke & Korycansky 1982; Antonucci et al. 1989).

in luminosity to the observed EELR which would clearly not be desirable.

5.2.2. On the detection of stellar continuum

For the case where hot stars alone ionize the foreground absorbers, we now estimate the implied stellar flux (or, equivalently, the Ly α equivalent-width) and compare it with the observations, beginning with the LAN.

Assuming a Salpeter IMF and the SED for an instantaneous burst of age 3.4 Myr (VM04), we find using MAPPINGS Ic that the rest-frame Ly α equivalent-width is EW^{rest}_{Ly α} = 190 $\epsilon_{\rm neb}$ Å. Defining the fraction of ionising photons reprocessed by the emission nebula as $\epsilon_{0.5}^{\rm neb}$ = $\epsilon_{\rm neb}/0.5$, we obtain that the (observer-frame) continuum flux is F^{obs}_c = 0.0105 { $\epsilon_{0.5}^{\rm neb}$ (1 + $z_{\rm e}$)}⁻¹ F^{obs}_{Ly α}Å⁻¹, where F^{obs}_{Ly α} is the observed line flux, corrected for absorption.

For the LAN, this implies a 5300 Å continuum of $F_c^{\rm obs}=9.4\times10^{-18}\,{\rm erg\,cm^{-2}\,s^{-1}\,\AA^{-1}},$ or equivalently, $8.8 \,\mu$ Jy. (The lens amplification was assumed to be the same for both the continuum and the lines). This flux is about 30 times higher than the upper limit set by Fig. 5 of Fosbury et al. (2003), of $\approx 0.3 \mu \text{Jy}$. A continuum was detected at longer wavelengths, but these authors report that it is consistent with being nebular in nature. As a solution, Fosbury et al. (2003) proposed a top-heavy IMF. Assuming a single $T_{\rm eff}$ SED of $80\,000\,{\rm K}$ (Fig. 1), we derive $EW_{Ly\alpha}^{rest} = 1335 \,\epsilon_{neb} \,\mathring{A}$, or a continuum of $1.3 \,\mu \text{Jy}(\epsilon_{0.5}^{\text{neb}} = 1)$. Even for a higher T_{eff} of $88\,000\,\text{K}$, we obtain a value of $1.1 \,\mu Jy$, similar to before. The increase of a factor 7–8 of the Ly α equivalent-widths provided by these two seds is therefore insufficient. A significantly hotter stellar SED is therefore required (Fosbury et al. proposed $\simeq 10^5$ K). Alternative explanations might consist of a peculiar dust distribution that preferentially absorbs the continuum and thereby increases the observed equivalentwidth or, as suggested by MV04, differential amplification of the lines and the continuum, by the gravitational lens. It is interesting to note that the Ly α -emitting 'blobs' associated with Lyman Break Galaxies likewise do not show the expected level for the stellar continuum (Steidel et al. 2000). For a possible explanation involving significant populations of metal-free stars, see Jimenez & Haiman (2006).

If we now turn to the two HzRGs, we place upper limits on the underlying stellar continua by defining limits on the contribution of hot stars to the EELR Ly α (which must be much smaller than the AGN contribution). Assuming the VM04 SED and the stellar contribution to be no more than 10% of the EELR, we derive continuum fluxes (at the observed Ly α wavelength) of 7.0×10^{-19} and 1.0×10^{-18} erg cm⁻² s⁻¹ Å⁻¹, for 0943–242 and 0200+015, respectively¹². These lie below the upper continuum limits

its of 3.1×10^{-18} and $2.6 \times 10^{-18} \,\mathrm{erg} \,\mathrm{cm}^{-2} \,\mathrm{s}^{-1} \,\mathrm{\AA}^{-1}$, respectively, as measured by van Ojik (1995). However, using recent VLT data from VIMOS-IFU (van Breukelen, Jarvis & Venemans 2005), one of us (MJ) reports detection of the underlying continuum in 0943-242 at the level of $1.7 \pm 0.9 \times 10^{-18} \,\mathrm{erg} \,\mathrm{cm}^{-2} \,\mathrm{s}^{-1} \,\mathrm{Å}^{-1}$, that is, less than a factor two above our limit. Vernet et al. (2001) reports on the measurement of a far-UV continuum in the form of "single peaked sources". This continuum, however, is 6.6% polarized near 1350 Å. Vernet et al. (2001) estimates that the AGN contributes between 27% and 66% of the continuum at 1500 Å. After allowing for a 20% contribution from the nebular continuum, these authors conclude that between 14 and 55% of the unpolarized continuum might be due to young stars. The continuum measured by MJ is then fortuitously consistent with our upper limit, since half of it or less is stellar in origin. We conclude that an instantaneous burst with a Salpeter IMF is thus a feasible source of ionization for HzRG absorbers. It would in any case be difficult to rule it out since continua much weaker than assumed in our test case (by a factor ~ 20) would still suffice to ionize the absorbers.

5.3. Summary of current constraints on HzRG halo ionization

To summarise the results of the previous two sections, we conclude that ionization by the MBR or by hot stars can satisfactorily reproduce the observed $N_{\rm CIV}/N_{\rm HI}$ ratios without recourse to excessive galaxy-to-galaxy metallicity variations. That was the aim of the photoionization modelling as defined in section 4.1.

On closer inspection, however, ionization by the MBR leads to excessively large radii for the absorbing shells and, by implication, to very large gas masses. This follows because the intensity of the MBR, J_{ν} , is not a free parameter so constraints on U translate directly into constraints on halo gas density. Given the latter, the observed requirement for a shell-like geometry translates directly into a minimum shell radius from the parent Hzrg. For both thick and thin absorbers, the minimum radii are of order several hundred kpc. This is hard to reconcile with the observed transition in radio source size between Hzrgs with and without strong absorption. Scaling as the square of the radius, the implied shell masses are also uncomfortably large.

The case of ionizing the absorber, but not the EELR, by hot stars circumvents the above problems, but at first sight raises separate issues of its own. The first is to ensure that these hot stars do not overproduce the Ly α emission, because in HzRGs the EELR is powered by AGN photoionization or jet interactions. In both 0200+015 and 0943-242 it was shown that Ly α emission from hot stars does not significantly contaminate the EELR emission. Potentially more serious is the apparent faintness of the stellar con-

weaker continuum is needed, as shown by the estimates of ${\rm Ly}\alpha$ luminosity reported in Sect. 5.2.2.

¹² It should be emphasized that these are maximum estimates of the stellar continuum. We recall that we can let the stellar continuum be much *weaker* than the test case explored in Sect. 5.2.1 and still have it ionize the shells. Furthermore, if $U \ll 0.1$, as considered for 0200+015 in Sect. 4.4.1, an even

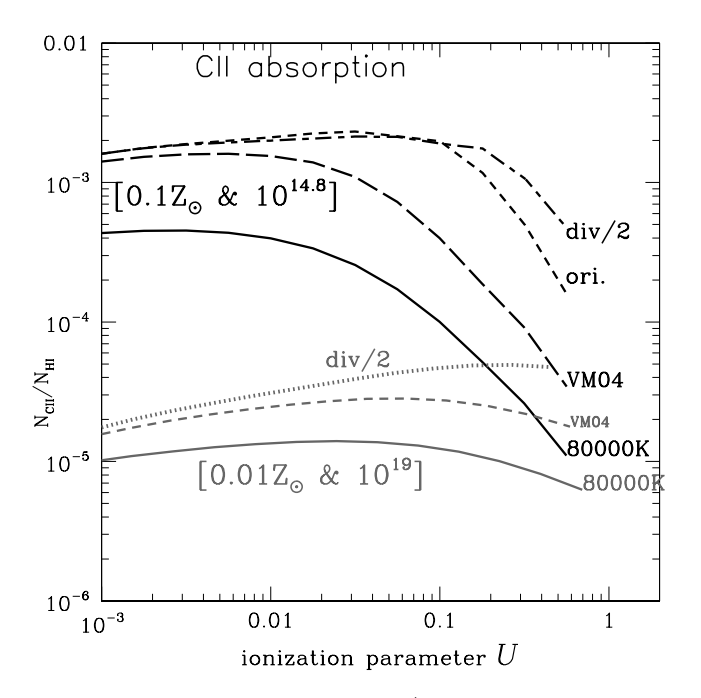


Fig. 7. The column ratio $N_{\rm CII}/N_{\rm HI}$ derived from photoionization by four different SEDs discussed in Sect. 4, as a function of U. The nomenclature and symbols have the same meaning as in Fig. 2.

tinuum, which is hard to explain away with peculiar dust geometries if the stars ionize gas in the direction of the observer. For the LAN Fosbury et al. (2003) appealed to hot stars and a top-heavy IMF; for the two Hzrgs, constraints on the continuum level below Ly α appear to be consistent with the levels expected from hot stars. For all these reasons, we thus favour hot stars as the more likely source of ionization for the Hzrg haloes and in the next section outline some new diagnostics to test this further.

6. New diagnostics for future observations

In order to resolve pending issues such as the size, masses and nature of the HzRG haloes, more extensive observations are needed and measurements of C IV in absorption in other HzRGs should be attempted. The detection of other absorption species would also help to break the Z-U degeneracy, as outlined below.

6.1. Absorption by lower ionization species: $C_{II}\lambda\lambda 1335$ and $Mg_{II}\lambda\lambda 2798$

It would be helpful to detect the absorption of other resonance lines in the spectra of HzRGs, particularly in the case of species of lower ionization than C IV. This could be used to confirm whether those H I absorbers without C IV absorption might simply correspond to shells of lower ionization (smaller U). Two candidate species are C II $\lambda\lambda$ 1335 and Mg II $\lambda\lambda$ 2798. We report calculations for these two resonance lines in Figs 7 and 8, assuming those SEDs that were most successful in reproducing the observed

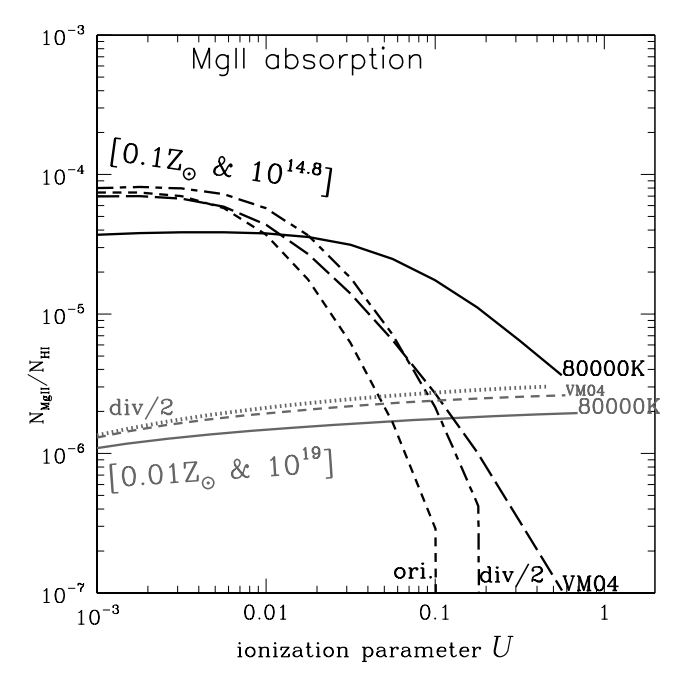


Fig. 8. The column ratio $N_{\rm MgII}/N_{\rm HI}$ derived from photoionization by four different SEDs discussed in Sect. 4, as a function of U.

 $N_{\rm CIV}/N_{\rm HI}$ ratios. Because both C II and Mg II are much weaker emission lines than Ly α , we consider it feasible to detect the corresponding absorption doublets only in the case of the thicker H I absorbers. For instance, for an absorber with $N_{\rm HI} \simeq 10^{19}\,{\rm cm}^{-2}$, we expect the C II and Mg II columns to be of order 10^{14} and $10^{13}\,{\rm cm}^{-2}$, respectively, assuming a metallicity of $0.01\,Z_\odot$. Interestingly, the behaviour of the $N_{\rm CII}/N_{\rm HI}$ and $N_{\rm MgII}/N_{\rm HI}$ ratios is relatively flat in the strong absorber case, with a dependence on U that is much weaker than was the case for C IV. This property would facilitate the determination of the gas metallicity. A possible strategy would be to use Mg II to ascertain the metallicity, and then use the appropriate C IV curve to constrain U.

6.2. Absorption by higher ionization species: $Ovi\lambda 1035$ and $Nv\lambda 1240$

McCarthy (1993) produced a composite optical-UV spectrum of 3CR and 1 Jy sources (redshifts up to 3) that is useful for estimating typical strengths of various emission lines. Their composite shows that the strongest resonance emission lines in radio-galaxies after Ly α and C IV $\lambda\lambda1549$ are (in order of decreasing flux) O VI $\lambda1035$, O IV+Si IV $\lambda1402$, N V $\lambda1240$, Mg II $\lambda\lambda2798$ and C II $\lambda\lambda1335$. Because O IV+Si IV $\lambda1402$ consists of a blend of two emission doublets, it is unlikely that the corresponding absorption lines could be disentangled. The other resonance lines left to consider are O VI and N V. In Fig. 9 and 10, we present the column ratios $N_{\rm OVI}/N_{\rm HI}$ and $N_{\rm NV}/N_{\rm HI}$, respectively, as a function of U. One can see from these figures that the ionization parameter could be considerably

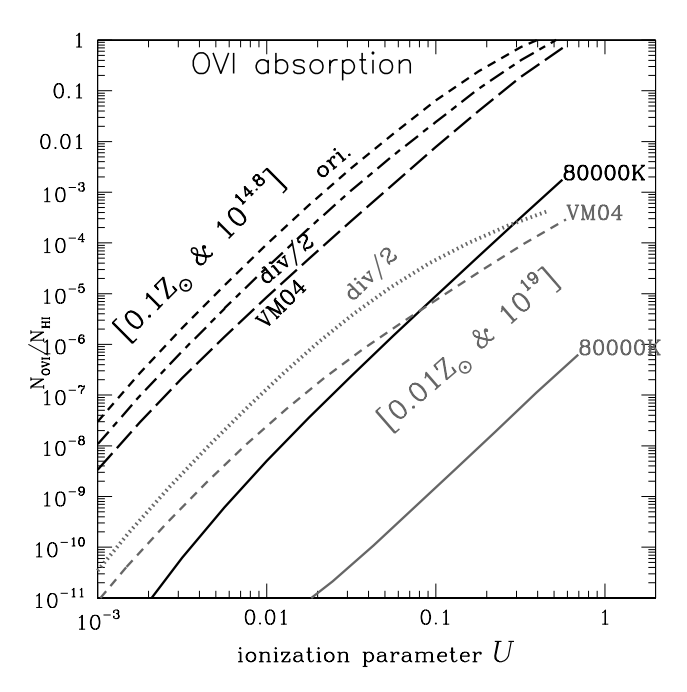


Fig. 9. The column ratio $N_{\rm OVI}/N_{\rm HI}$ derived from photoionization by four different SEDs discussed in Sect. 4, as a function of U.

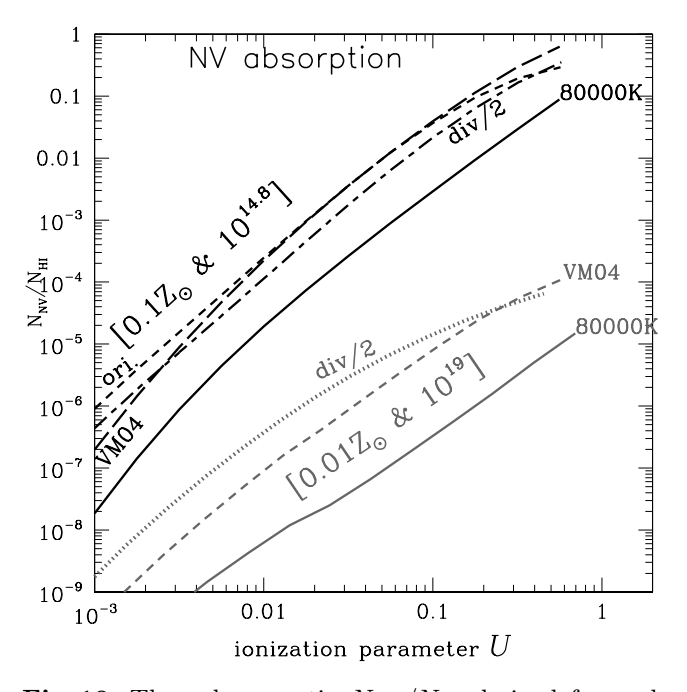


Fig. 10. The column ratio $N_{\rm NV}/N_{\rm HI}$ derived from photoionization by four different SEDs discussed in Sect. 4, as a function of U.

better constrained if data on these resonance lines were obtained. Thus, obtaining high-resolution optical spectra over all emission lines is essential to better constrain the properties of these haloes.

Acknowledgements. One of the authors (LB) acknowledges financial support from CONACyT grant 40096-E and the

UNAM PAPIIT grants 113002 and 118601. RJW and MJJ acknowlege the support of PPARC PDRAs. RAEF is affiliated to the Research and Science Support Department of the European Space Agency. Diethild Starkmeth helped us with proof-reading. We acknowledge the technical support of Liliana Hernández and Carmelo Guzmán for configuring the Linux workstation Deneb.

References

Adelberger, K. L., Shapley, A. E., Steidel, C. C., Pettini, M., Erb, D. K., & Reddy, N. A. 2005, ApJ, 629, 636

Anders, E., & Grevesse, N. 1989, Geochim. Cosmochim. Acta, $53,\ 197$

Antonucci, R. R. J., Kinney, A. L., & Ford, H. C. 1989, ApJ, 342, 64

Antonucci, R. 1993, ARA&A, 31, 473

Barthel, P. D. 1989, ApJ, 336, 606

Beckman, J. E., Rozas, M., Zurita, A., Watson, R. A., & Knapen, J. H. 2000, AJ, 119, 2728

Binette, L., Wang, J. C. L., Zuo, L., & Magris, C. G. 1993, AJ, 105, 797

Binette, L., Dopita, M.A., Tuohy, I.R., 1985, ApJ, 297, 476 Binette, L., Kurk, J. D., Villar-Martín, M., Röttgering, H. J. A.

2000, A&A, 356, 23 (B00)
Binette, L., Groves, B., Villar-Martín, M., Fosbury, R. A. E.,
& Axon, D. J. 2003, A&A, 405, 975 (BG03)

Cerviño, M., Mas-Hesse, J. M., & Kunth, D. 2004, available at http://www.laeff.esa.es/users/mcs/SED (CMK04)

Cooke, A. J., Espey, B., & Carswell, R. F. 1997, MNRAS, 284, 552

Dopita, M. A., & Sutherland, R. S. 1996, ApJS, 102, 161

Fardal, M. A., Giroux, M. L., & Shull, J. M. 1998, AJ, 115, 2206 (FGS)

Ferruit P., Binette, L., Sutherland, R. S., Pécontal, E. 1997, A&A, 322, 73

Fosbury, R. A. E., Villar-Martín, M., Humphrey, A., et al. 2003, ApJ, 596, 797

Giammanco, C., Beckman, J. E., & Cedrés, B. 2005, A&A, 438, 599

Haardt, F., & Madau, P. 1996, ApJ, 461, 20

Haas, M., Siebenmorgen, R., Schulz, B., Krügel, E., & Chini, R. 2005, A&A, 442, L39

Heckman, T. M., Miley, G. K., van Breugel, W. J. M., & Butcher, H. R. 1981, ApJ, 247, 403

Holden, B. P., Stanford, S. A., Rosati, P., et al. 2001, AJ, 122, 629

Jarvis, M. J., Wilman, R. J., Röttgering, H. J. A., & Binette, L. 2003, MNRAS, 338, 263 (J03)

Jimenez, R., & Haiman, Z. 2006, Nature, 440, 501

Krause, M. 2002, A&A, 386, L1

Krause, M. 2005, A&A, 436, 845

Kriss, G. A., et al. 2001, Science, 293, 1112

McCarthy, P. J. 1993, ARA&A, 31, 639

Oke, J. B., & Korycansky, D. G. 1982, ApJ, 255, 11

Pettini, M., Shapley, A. E., Steidel, C. C., Cuby, J.-G., Dickinson, M., Moorwood, A. F. M., Adelberger, K. L., & Giavalisco, M. 2001, ApJ, 554, 981

Relaño, M., Peimbert, M., & Beckman, J. 2002, ApJ, 564, 704
Röttgering, H. J. A., Hunstead, R. W., Miley, G. K., van Ojik,
R., Wieringa, M. H. 1995, MNRAS, 277, 389

Röttgering, H., & Miley, G. 1997, in The Early Universe with the VLT, Springer, Berlin, ed. J. Bergeron, p. 285

- Schaerer, D. 2002, A&A, 382, 28
- Shields, G. A. & Searle, L. 1978, ApJ, 222, 821
- Smette, A., Heap, S. R., Williger, G. M., Tripp, T. M., Jenkins, E. B., & Songaila, A. 2002, ApJ, 564, 542
- Steidel, C. C., Adelberger, K. L., Shapley, A. E., Pettini, M., Dickinson, M., & Giavalisco, M. 2000, ApJ, 532, 170
- Telfer, R. C., Kriss, G. A., Zheng, W., Davidsen, A. F., & Tytler, D. 2002, ApJ, 579, 500
- van Breukelen, C., Jarvis, M. J., & Venemans, B. P. 2005, MNRAS, 359, 895
- van Ojik R., Röttgering, H. J. A., Miley, G. K., Hunstead, R. W. 1997, A&A, 317, 358 (VO97)
- van Ojik R. 1995, Ph. D. thesis, University of Leyden, Holland van Breugel, W. J. M., Miley, G. K., McCarthy, P. J., & Spinrad, H. 1997, The Hubble Space Telescope and the High Redshift Universe, 369
- Vernet, J., Fosbury, R. A. E., Villar-Martín, M., Cohen, M. H., Cimatti, A., di Serego Alighieri, S., & Goodrich, R. W. 2001, A&A, 366, 7
- Villar-Martín, M., Cerviño, M., & González Delgado, R. M. 2004, MNRAS, 355, 1132 (VM04)
- Wilman, R. J, Jarvis, M. J., J., Röttgering, H. J. A., & Binette, L. 2004, MNRAS, 351, 1109 (W04)
- Wilman, R. J., Gerssen, J., Bower, R. G., Morris, S. L., Bacon, R., de Zeeuw, P. T., & Davies, R. L. 2005, Nature, 436, 227
- Zurita, A., Beckman, J. E., Rozas, M., & Ryder, S. 2002, A&A, 386, 801